

***In vitro* in-stent restenoses evaluated by 3D ultrasound**

Myriam Lécart and Marie-Hélène Roy Cardinal

Laboratory of Biorheology and Medical Ultrasonics, University of Montreal Hospital Research Center (CRCHUM), 2099 Alexandre de Sève (room Y-1619), Montréal, Québec H2L 2W5, Canada and Institute of Biomedical Engineering, University of Montreal, Montréal, Québec H3T 1J4, Canada

Zhao Qin

Laboratory of Biorheology and Medical Ultrasonics, University of Montreal Hospital Research Center (CRCHUM), 2099 Alexandre de Sève (room Y-1619), Montréal, Québec H2L 2W5, Canada

Gilles Soulez

Department of Radiology, University of Montreal Hospital, Montréal, Québec H2L 4M1, Canada and Department of Radiology, Radio-Oncology and Nuclear Medicine, University of Montreal, Montréal, Québec H3T 1J4, Canada

Guy Cloutier^{a)}

Laboratory of Biorheology and Medical Ultrasonics, University of Montreal Hospital Research Center (CRCHUM), 2099 Alexandre de Sève (room Y-1619), Montréal, Québec H2L 2W5, Canada; Department of Radiology, Radio-Oncology and Nuclear Medicine, University of Montreal, Montréal, Québec H3T 1J4, Canada; and Institute of Biomedical Engineering, University of Montreal, Montréal, Québec H3T 1J4, Canada

(Received 11 March 2008; revised 10 December 2008; accepted for publication 11 December 2008; published 23 January 2009)

The purpose of this study was to quantify in-stent restenoses with 3D B mode and power Doppler ultrasound (U.S.) imaging. In-stent restenoses were mimicked with vascular phantoms in which a nonferromagnetic prototype stent (Boston Scientific) and a ferromagnetic clinical stainless steel stent (Palmaz P295) were embedded. Each phantom had an 80% in-stent stenosis and a 75% stenosis located outside the stent. These phantoms were compared to a reference phantom reproducing both stenoses without stent. Data sets of 2D cross-sectional U.S. images were acquired in freehand scanning using a magnetic sensor attached to the U.S. probe and in mechanical linear scanning with the probe attached to a step motor device. Each 2D image was automatically segmented before 3D reconstruction of the vessel. Results indicate that the reference phantom (without stent) was accurately assessed with errors below 1.8% for the 75% stenosis and 3.2% for the 80% stenosis in both B mode and power Doppler for the two scanning methods. The 80% in-stent stenoses in Boston Scientific and Palmaz stents were, respectively, evaluated at 73.8(\pm 3.2)% and 75.8(\pm 3)% in B mode and at 82(\pm 2.5)% and 86.2(\pm 6.4)% in power Doppler when freehand scans were used. For comparison, when linear scans were selected, in-stent stenoses in the Boston Scientific or Palmaz stent were, respectively, evaluated at 77.4(\pm 2.0)% and 73.8(\pm 2.5)% in B mode and at 87.0(\pm 1.3)% and 85.6(\pm 5.8)% in power Doppler. To conclude, 3D freehand U.S. is a valuable method to quantify in-stent restenoses, particularly in B mode. It is thus hoped that, in the clinical setting, noninvasive 3D U.S. may provide sufficient precision to grade in-stent restenoses. © 2009 American Association of Physicists in Medicine. [DOI: 10.1118/1.3062944]

Key words: 3D ultrasound imaging, freehand scanning, phantoms, electromagnetic tracking device, in-stent restenosis

I. INTRODUCTION

Currently, digital subtraction angiography is the gold standard procedure to image in-stent restenosis, but it is invasive. Arterial in-stent restenoses have been quantified hemodynamically using duplex ultrasound (U.S.). The Doppler peak systolic velocity (PSV) and PSV ratio between two sites (PSV at the stenosis divided by PSV in a presumably normal segment) allowed the detection of in-stent restenoses. However, depending on the operator and ultrasound scanners, different thresholds of velocities or PSV ratios can be proposed for the same vascular territory. As an example, PSV thresh-

olds varying between 150 cm/s (Ref. 1) and 300 cm/s (Ref. 2) have been suggested to detect moderate-to-severe in-stent stenoses after carotid stenting.³ Current knowledge suggests the need for a redefinition of diagnostic velocity thresholds following stenting.

Stent imaging with computed tomography (CT) angiography is afflicted by artificial narrowing of the in-stent lumen and beam hardening artifacts that may hamper restenosis assessment.⁴ Magnetic resonance (MR) angiography is also limited by susceptibility and radio-frequency shielding artifacts related to the metallic composition of the stent.⁵ A morphological characterization using B-flow imaging⁶ similar to

2D and 3D MRA and CTA acquisitions could be more objective and reproducible for the evaluation of in-stent restenoses.

Three-dimensional U.S. appears nowadays as a good alternative to CT and MR, especially in assessing peripheral vessels.^{7,8} Ultrasonography is advantageous since it is inexpensive and noninvasive (no hazard related to ionizing radiation, iodine, or gadolinium contrast agent injection) and because it is possible to acquire images in real time. 3D U.S. compensates the disadvantages of 2D U.S. that is limited by the 2D sight; it also allows precise measurements of an organ's volume and the visualization of anatomy in 3D.⁹ Three-dimensional ultrasonography requires three stages:¹⁰ data acquisition, 3D reconstruction, and visualization. Within the past few years, 3D U.S. methods using B mode or power Doppler angiography (PDA)^{8,11–13} have been successfully used to quantify models of stenotic arteries. However, the presence of an endoprosthesis such as a metallic stent is suspected to create artifacts on 2D U.S. images and 3D reconstructions, increasing the difficulty to accurately evaluate the degree of in-stent restenosis.

Although 3D Doppler ultrasound has already been used in a clinical setting to detect in-stent stenosis after carotid stenting,⁶ systematic evaluation of the influence of stent design and 3D acquisition protocol on stenosis measurement error have not been investigated. The first objective of this study was to determine if stents have an impact on the diagnosis with 3D ultrasonography. Furthermore, because electromagnetic tracking devices (commonly used with freehand U.S. imaging systems) are very sensitive to ferromagnetic metals, the second objective was to compare 3D reconstructions of ferromagnetic and nonferromagnetic stents using such a positioning device.

II. MATERIALS AND METHODS

II.A. Vascular phantoms

The study was performed on vascular phantoms. Three phantoms with double arterial stenoses of 75% and 80% area reductions were compared: a reference phantom without stent, a phantom with a prototype stent (Boston Scientific Corporation, Munich, Germany), and another one with a stent used in clinical practice (Palmaz, Cordis, Johnson&Johnson, Miami Lakes, FL), both stents covering the 80% stenosis.

II.A.1. Phantom fabrication

A cylindrical vessel containing both stenoses (75% and 80%), made with a cerrowal shank, was put in a polyethylene box that was subsequently filled with a tissue-mimicking gel composed of water (89%), glycerol (8%), and agar (3%). The solidified gel had similar acoustic properties (attenuation and sound velocity) as human tissues.¹⁴ The wall-less lumen was created by liquefying and removing the shank by heating the phantom above the melting point of cerrowal. The wall-less vessel avoided diffraction of the U.S. beam, which may be encountered when using tubelike artery models.¹⁵ Each

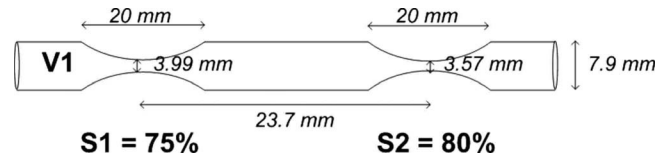


FIG. 1. Phantom lumen dimensions (at scale). V1 indicates the proximal segment of the artery and S1 and S2, respectively, represent the 75% and 80% area reduction stenoses.

vessel contained two adjacent stenoses as shown in Fig. 1. Two phantoms were created with the 80% stenosis covered by a stent. When pouring the liquid gel in the phantom during the fabrication process, it passed through the mesh of the stent before solidifying, filling the space around the cerrowal shank. The phantom identified as the “Boston phantom” included a prototype MR compatible stent, whereas we used a commercially available Palmaz stent for the “Palmaz phantom.” Vascular phantoms were kept in water to prevent drying and, consequently, to preserve the initial dimension of the lumen.

II.A.2. Phantom dimensions

All phantoms had identical stenosis severities and dimensions. The diameter of the nonobstructed lumen (V1 on Fig. 1) was 7.9 mm. The length of each stenosis, between the proximal and distal segments with a diameter equivalent to V1, was 20 mm. The distance between the centers of each cosine-shaped stenosis was 23.7 mm. We used similar phantoms in a recent flow modeling and experimental study.¹⁶

II.A.3. Stent characteristics

The Boston Scientific stent prototype is nonferromagnetic, has an open cell design, and was expanded to a diameter of 8 mm giving a length of 16 mm [Fig. 2(a)]. It is made of 99% niobium and 1% zirconium; its design is similar to the BSC liberté stent (Boston Scientific, Natick, MA). On the contrary, the Palmaz balloon expandable stent is ferromagnetic and made of stainless steel and has a closed cell design. We used a Palmaz P295 stent (Cordis-Johnson&Johnson, Warren, NJ) expanded to 8 mm giving a length of 24 mm [Fig. 2(b)]. We experimentally measured with a camera and

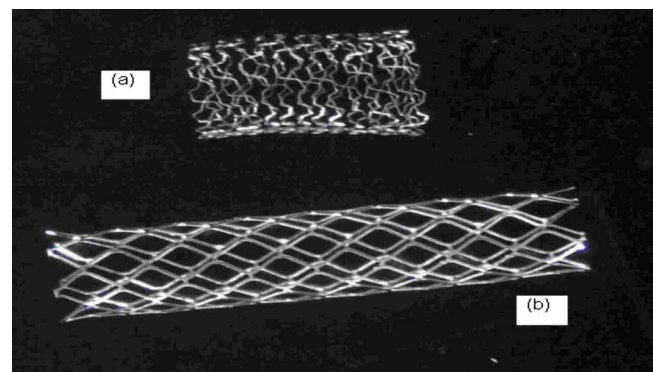


FIG. 2. (a) Boston Scientific stent prototype; (b) Palmaz stent.



FIG. 3. Ultrasound probe fixed on a step motor to perform a linear scan in cross-sectional view of the vessel embedded within the phantom box.

an image processing software the free cell area and (free cell/metal) area ratios ($n=10$ cells). They were $10(\pm 0.9)$ mm² and 4.5 for the Boston Scientific stent and $6.1(\pm 0.1)$ mm² and 4.8 for the Palmaz one.

II.B. Data acquisition methods

Two scanning methods were used to produce 3D U.S. images of each phantom. A linear scan with the U.S. probe attached to a step motor, as in Refs. 8 and 11, was first performed. Although it is very constraining for clinicians, this scanning technique is considered as a gold standard for 3D ultrasonography because of its accuracy.⁸ The second approach was a 3D freehand U.S. system based on an ac electromagnetic tracking device. In both systems, the main equipments (U.S. scanner, U.S. probe, video acquisition card) and settings were kept the same. U.S. images were captured on a computer with a video acquisition board (ATI TV Wonder Pro, ATI Technologies, Santa Clara, CA) connected to the standard S-video output of the clinical U.S. scanner (Vivid Five, General Electric, Chicago, IL). Ultrasound images were acquired with a 10 MHz linear array transducer (FLA 10). The size of the digitized U.S. images was 576×768 pixels, with a pixel size of 0.16 mm. Images were acquired in B mode and in PDA mode at a frame rate of 6 Hz (maximal value of the ATI video card). For power Doppler recordings, a pulse repetition frequency of 750 Hz was used and the blood mimicking fluid (1 l of water mixed with 250 ml of corn starch particles and 180 ml of glycerol) was circulated under a steady flow rate of 500 ml/min. Salt (9 g) was added to the mimicking fluid to allow recording of the flow rate with an electromagnetic flow meter (Cliniflow II, Carolina Medical, King, NC). All experiments were done at room temperature.

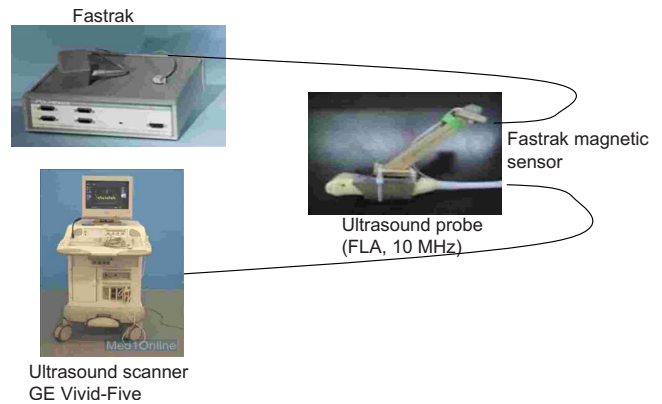


FIG. 4. Description of the 3D freehand ultrasound acquisition system.

II.B.1. Linear scanning method

The U.S. probe was attached to a step motor (see Fig. 3), which allowed a linear and discrete movement of the probe with a fixed step (0.52 mm) and angle (90° in B mode and 80° in PDA). The step motor total displacement was 92 mm with the velocity set to 3 mm/s. The gradual evolution of the vessel was clearly seen at this velocity, making the automatic segmentation of 2D U.S. frames possible. A total of 184 digitized cross-sectional images were acquired in approximately 30 s.

II.B.2. Freehand scanning method

Three-dimensional freehand U.S. comprises the acquisition of a sequence of 2D images with their positions recorded with a tracking device and the reconstruction of the 3D volume. The freehand U.S. system (Fig. 4) was composed of the ac electromagnetic tracking device (Fastrak, Polhemus, Colchester, VT) combined with the U.S. scanner. Although the Fastrak is sensitive to ferromagnetic metals, this type of sensor is flexible, inexpensive, and easy to use for clinical applications. To minimize electromagnetic interferences produced by the U.S. probe,¹⁷ the sensor was mounted on a wooden support and located approximately 10 cm away from the U.S. transducer. Also, the operating range of the freehand system (distance between sensor and transmitter) was kept under 1 m, as recommended by the manufacturer. The tracking device was connected to a computer using an RS 232 cable. The U.S. data acquisition, sensor position, and orientation were synchronized by a software (STRADWIN) developed by Prager *et al.*¹⁸ This software associates the coordinates of the Fastrak sensor with each of the U.S. image recorded with the video acquisition card. In B-mode scans, the probe was manually positioned close to perpendicular to the phantom, whereas in power Doppler scans, the angle was approximately 80° to detect the flow.

A calibration step is required to accurately place a pixel of the U.S. image in the 3D space. The aim of the spatial calibration is to determine the transformation (a rotation, a translation, and sometimes a scale modification) between the origin of the sensor attached to the probe and the U.S. image itself. The STRADWIN software was used to do the spatial

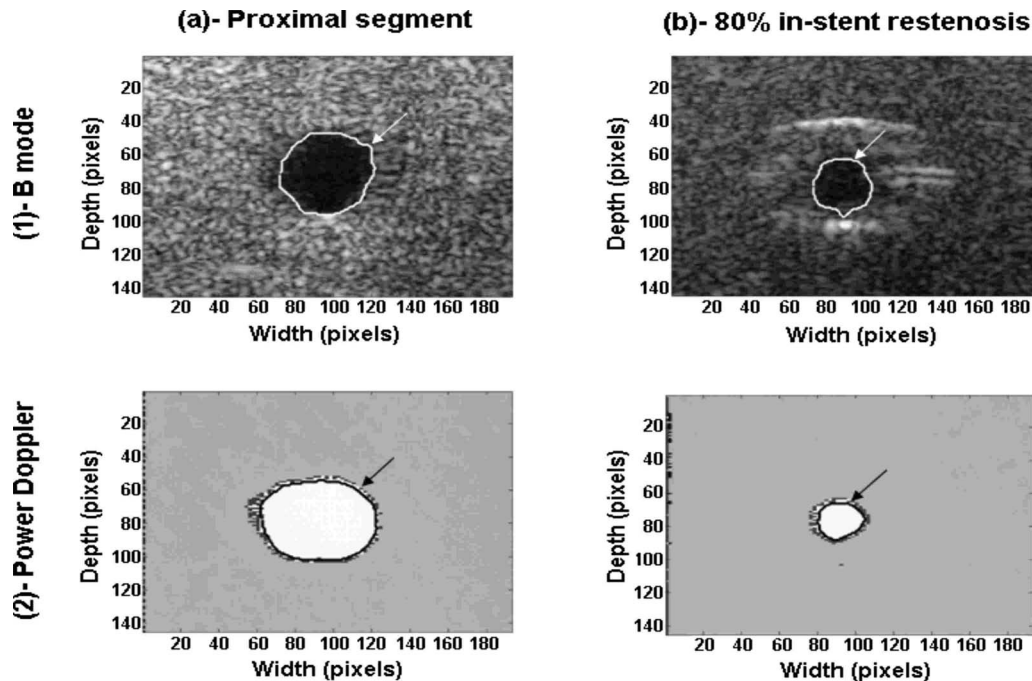


FIG. 5. Segmentation of the lumen for the Boston Scientific phantom: (a) proximal segment and (b) in the throat of the 80% in-stent restenosis for (1) B mode and (2) power Doppler scans (flow rate=500 ml/min). The segmented contours are indicated by arrows.

calibration of the system based on the equations of Prager *et al.*¹⁹ It estimates the transformation matrix necessary to locate each 2D U.S. frame in the imaging volume. Therefore, the accuracy of the 3D reconstruction depends largely on the accuracy of the calibration. A planar calibration phantom²⁰ made of a Plexiglas plate at the bottom of a water bath was used. This phantom, when imaged with U.S., provides line images. The calibration was thus quick, automatic, and reproducible^{19,20} because the line was automatically detected in each U.S. image by a minimization algorithm implemented under STRADWIN.

II.C. Segmentation, 3D reconstruction, and visualization

II.C.1. Segmentation

The cross-sectional images acquired with both 3D scanning techniques were segmented using the same automated 2D fast-marching method adapted from Refs. 21 and 22 to detect the lumen boundary on each frame of the sequence. B-mode images were segmented as they were acquired [Fig. 5-1], whereas PDA images were first transformed to gray scale images [Fig. 5-2]. The segmentation was based on a combination of contour and region information, namely, the image intensity gradient and the gray level probability density functions (PDFs) of the lumen and surrounding tissue-mimicking medium. The gray level PDFs were automatically detected for each sequence to take into account the intensity variations between acquisitions. To preserve the 3D continuity of the lumen, the segmentation of each image was initialized with the detected lumen contour on the previous frame of the sequence, except for the first frame that was initialized manually.

II.C.2. 3D reconstruction and visualization

For the linear scanning method in B mode, the acquired 2D images were simply stacked to reconstruct the volume because they were acquired perpendicularly to the vessel axis with a fixed step. In power Doppler, scans were performed with an angle between the vessel axis and the ultrasound beam. The segmented contours were thus projected on the plane perpendicular to the vessel axis to compensate for the acquisition angle in Doppler mode. The same reconstruction method was used for the B-mode and PDA acquisitions with the freehand scanning approach. Segmented contours were positioned in space using the calibration parameters (calibration matrix and scale factors obtained with STRADWIN) and the acquired image coordinates.¹⁹

II.C.3. Determination of the percentages of area reduction restenosis

In linear scan mode, vessel areas were computed directly with the detected B-mode boundaries and reoriented PDA contours. For the freehand method, the scan was done freely, which means that the acquired images were not parallel, giving different probe/vessel angles from one image to another. Moreover, the displacement step between images was not constant. Each contour point was thus reoriented around the principal axis of the scan. A principal component analysis (PCA) of the x , y , and z coordinates of all contours was first performed to determine the principal x' , y' , and z' axes. The axes were relabeled to make the z' axis correspond to the largest eigenvalue of the PCA. The contours were then projected onto the (x', y') plane perpendicular to the z' axis

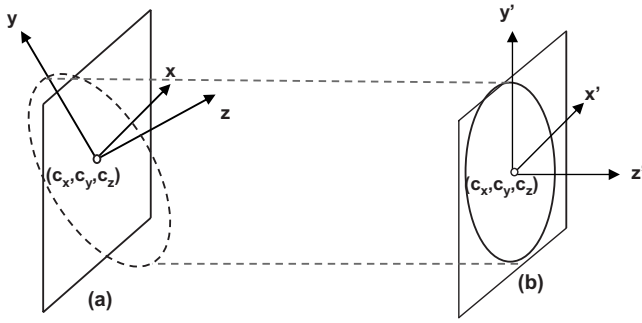


FIG. 6. Projection planes of (a) acquired and (b) orthogonally reconstructed images. (c_x, c_y, c_z) represents the geometric center of the contour, (x, y) is the plane of the initial contour, (x', y') is the projection plane, z is the axis of the initial contour perpendicular to (x, y) , and z' corresponds to the artery axis of the reoriented contour perpendicular to (x', y') .

and centered on the geometric center (c_x, c_y, c_z) of the contour (Fig. 6). The area of each contour in the projection plane was then computed.

For each phantom, the stenosis severity was evaluated as follows: ten scans were consecutively acquired for each 3D method in both B-mode and power Doppler imagings. The acquired images were segmented and reconstructed in 3D according to the previously described method. The degree of stenosis was evaluated according to the following formula:

$$S_{\text{stenosis}} = 100 \times \left(1 - \frac{S_{\text{stenosis, min}}}{S_{\text{stenosis, max}}} \right), \quad (1)$$

where $S_{\text{stenosis, min}}$ is the minimum lumen area in the throat of the stenosis (S1 or S2) and $S_{\text{stenosis, max}}$ is the mean of 20 consecutive lumen areas in the proximal segment (V1). The degree of restenoses presented in this study was calculated as the mean stenosis severity of the ten U.S. scans.

The 3D reconstructions were also quantitatively compared to the geometrical dimensions of the phantom. The vessel lumen along the z axis was described by the following analytical equation:¹⁶

$$r = R - e \left(\frac{1}{2} \cos \left(\frac{2\pi}{L_s} (z - Z) + \frac{\pi}{2} \right) \right), \quad (2)$$

where r is the radial coordinate of the vessel, R is the non-constricted vessel radius ($R=3.95$ mm), $e=R \times (1 - (1 - p/100)^{1/2})$ is the maximum reduction in the vessel radius at the stenosis, p is the percentage of area reduction in the lumen, $L_s=20$ mm is the stenosis length, Z is the axial position of the stenosis center from the beginning of the vessel, and z is the axial position along the curvature of the stenosis ($Z - L_s/2 \leq z \leq Z + L_s/2$) from the beginning of the vessel segment. Errors reported in this study were computed with the ground truth stenosis severities of 75% and 80% and thus include the reported phantom manufacturing error of $0.4(\pm 1.3)\%$.²³

II.D. Statistical analyses

To determine the impact of phantoms, stents, and imaging mode on the reconstructed volumes, a three-way analysis of variance with multiple comparisons performed with the Tukey method (ANOVA, SIGMASTAT, version 3.11, Systat Software, San Jose, CA) was used for the linear scanning method. To compare the accuracy of the linear and freehand scanning methods and to specify the impact of the method, another three-way analysis of variance with multiple comparisons performed with the Tukey method on each stenosis was used. These statistical tests were done using raw data before averaging. The level of statistical significance was fixed at $p < 0.05$.

III. RESULTS

III.A. 3D reconstructions

Ten reconstructions of the Boston, Palmaz, and reference phantoms were performed in B mode and in PDA with the linear scanning and freehand methods. Figure 7 shows examples of 3D reconstructions and corresponding errors in mm [Figs. 7(a) and 7(b), respectively] of the Boston phantom in B mode using the linear [Fig. 7-1] and the freehand [Fig. 7-2] scanning methods. Similar reconstruction results were achieved in power Doppler and with the other phantoms (Boston phantom in PDA and reference and Palmaz phantoms; results not shown).

To estimate the spatial calibration error in the experimental environment, ten calibrations were done using the STRADWIN software with an U.S. image depth setting of 4.5 cm (the same as used for the scanning of phantoms). For each calibration, 40 images were saved to compute the spatial calibration matrices. The average root-mean-square (rms) error of all ten calibrations was 1.0 ± 0.1 mm, which is smaller than the largest errors noted in Fig. 7(b).

Qualitatively, the 3D reconstructions using the freehand data acquisition method seemed less regular than those obtained using the mechanical linear scanning. Freehand scanned phantoms did not appear axisymmetric and the central axis of the lumen did not seem perfectly straight. However, the diameter quantification error of the degrees of stenosis and in-stent restenosis errors computed from the 3D reconstructions were less than 1 mm [Fig. 7(b)] independently of the scanning method. The largest errors close to 2 mm were at the stent end points [Fig. 7(b)].

III.B. Quantitative comparison of stenosis area reduction severities

Figure 8 shows the evolution of the lumen area percentages (compared to $S_{\text{stenosis, max}}$) along the artery axis (mean of ten scans) for the mechanical linear scanning method and for the freehand method. The most severe stenosis was defined as the origin of the artery axis. In B mode and PDA, using both scanning methods, the lumen areas of the three phantoms did not perfectly follow the theoretical curve, labeled Gt and given by Eq. (2). In the throat of both stenoses, the lumen areas were more biased in power Doppler than B

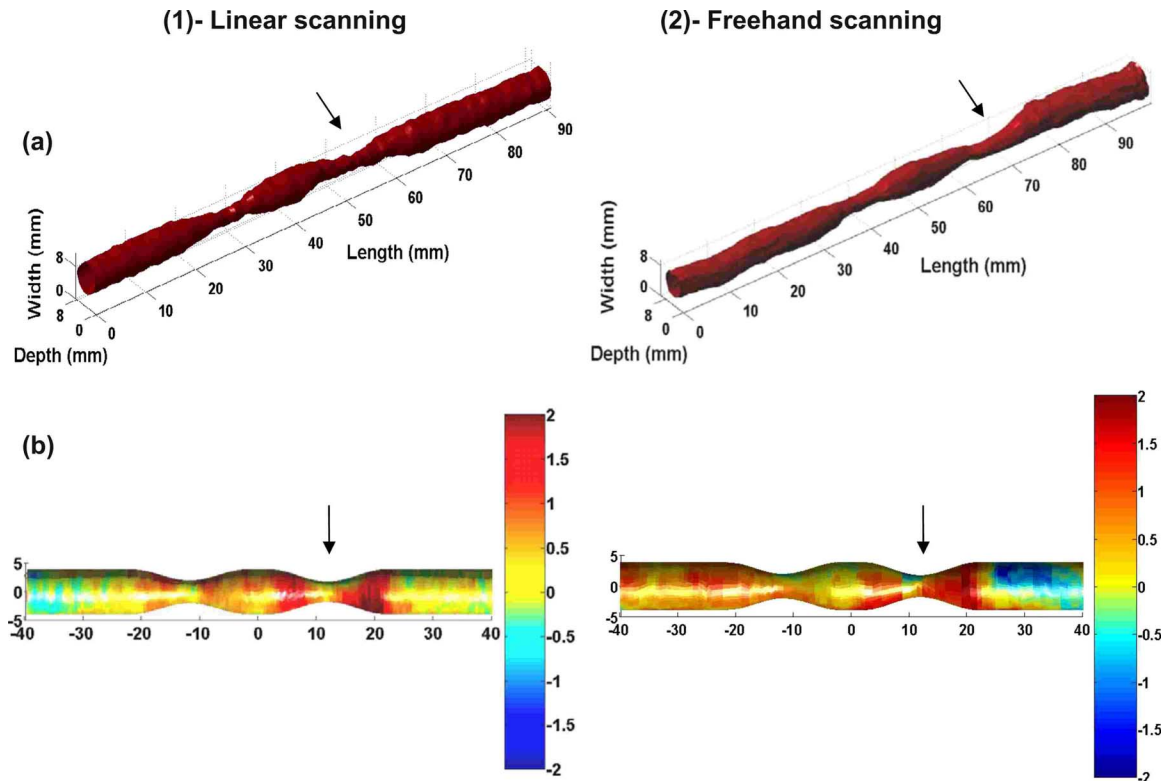


FIG. 7. (a) 3D reconstruction and (b) its error for the Boston Scientific phantom in B mode using (1) the mechanical linear scanning method and (2) the freehand scanning method. The errors in (b) as indicated by the color bar are in millimeters; they were generated from the ground truth equation of the lumen. The position of the stent on each reconstruction is indicated by an arrow.

mode and overestimated. In addition, for the 80% stented stenosis, higher errors were obtained for the Palmaz stent.

Table I summarizes the percentages of area reduction differences with respect to the ground true values at S1 and S2 obtained for ten U.S. scans in B mode and PDA using linear and freehand scanings. Absolute errors on S1 and S2 for linear scanning ranged, respectively, between 0.1% and 1.8% and between 0.6% and 7.0%. The freehand method resulted in errors varying between 0.1% and 6.7% for the stenosis S1 and between 0.4% and 6.2% for S2.

III.C. Impact of the phantom fabrication, imaging mode, and presence of stent on stenosis severities

Before further analyzing our results, the reproducibility of the fabrication process was verified, although high accuracies in the phantom lumen dimensions were reported earlier by our group.²³ The impact of phantoms was defined by the ability to quantify the S1 stenosis (no stent) in B mode when using the reference linear scanning method. According to Table I, the reference, Boston, and Palmaz phantom errors on S1 were, respectively, 0.1%, 1.3%, and 1.7% (no statistical differences, $p=0.147$).

The impact of the imaging mode was first evaluated with the linear scan reconstructions. There were statistically significant differences between B mode and PDA for the quantification of S1 and S2 stenoses for each phantom ($p < 0.05$). Three-dimensional B-mode imaging overestimated the severity of S1 stenoses by a maximum of 1.7% and un-

derestimated S2 in-stent stenoses by 2.6% for the Boston stent and 6.2% for the Palmaz stent. At the opposite, 3D PDA underestimated S1 stenoses by a maximum of 1.8% and overestimated S2 in-stent stenoses by 7% for the Boston and 5.6% for the Palmaz stent.

Using linear scans, the difference between in-stent stenosis (S2) values among the different stents was statistically significant in B mode ($p < 0.05$) but not in PDA ($p=0.453$). Indeed, using 3D B-mode ultrasound, the S2 in-stent restenoses within the Boston nonferromagnetic stent and the ferromagnetic Palmaz one were significantly underestimated by 2.6% and 6.2%, respectively. On the contrary, using 3D PDA, in-stent restenoses were both significantly overestimated by 5.6%–7%. Using the freehand method, the overestimation on PDA acquisition was more pronounced with the Palmaz (6.2%) than with the Boston (2%) ($p < 0.05$) and no difference on stenosis underestimation was observed with B-mode acquisitions.

The impact of the scanning method was quantified by comparing freehand scans with linear scans in B mode and in power Doppler for each stenosis. Using 3D B-mode imaging, no statistically significant difference was found between the scanning methods to quantify S1 ($p=0.954$) as well as the in-stent stenosis S2 ($p=0.238$). However, statistically significant differences were found with 3D PDA. Indeed, S1 stenosis of the Palmaz phantom was, respectively, quantified with 1.5% and 6.7% errors with the linear and freehand scans ($p < 0.001$). Furthermore, the S2 in-stent restenosis of the

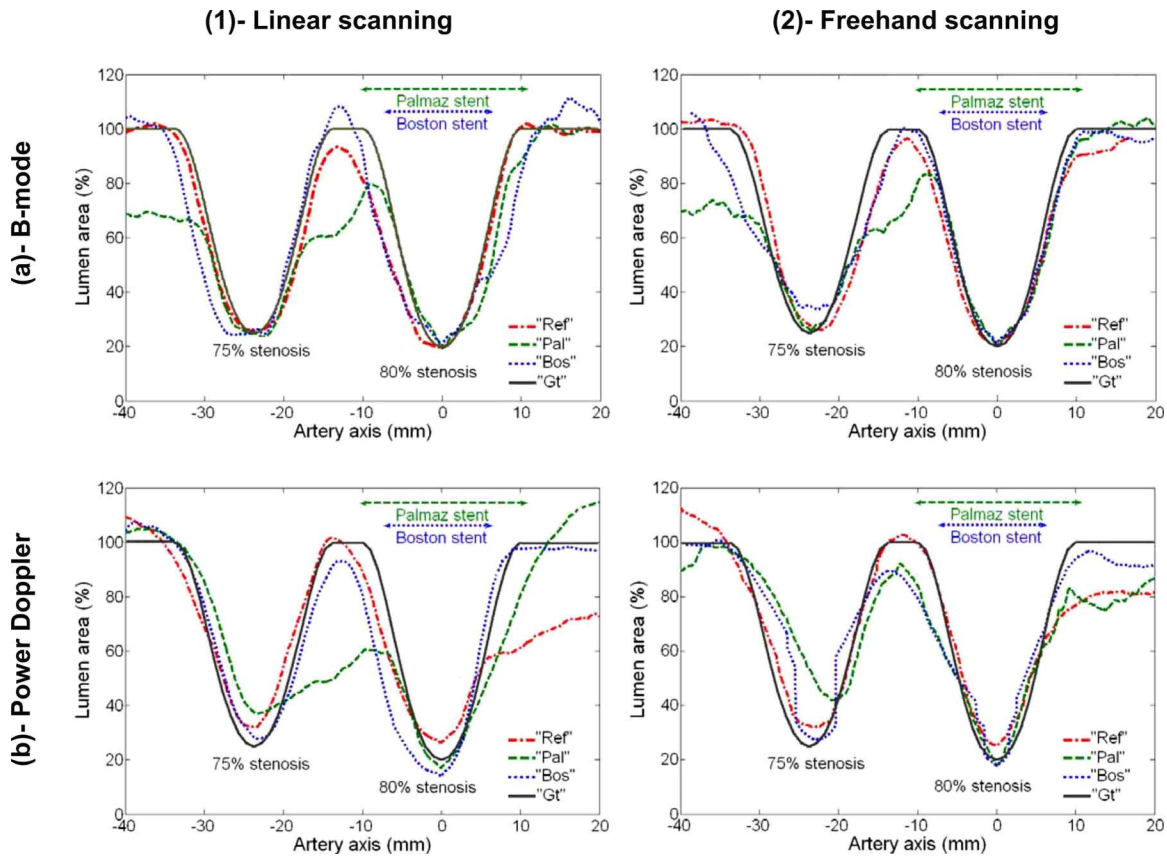


FIG. 8. Quantitative comparisons of 3D reconstructions for the reference phantom (Ref), the Palmaz phantom (Pal), and the Boston Scientific phantom (Bos) by using (1) the mechanical linear scanning method and (2) the freehand scanning method: (a) in B mode and (b) in power Doppler. Arrows indicate approximately the position of the two stents (the Palmaz was longer than the Boston Scientific one). The label Gt represents the ground true given by Eq. (2).

TABLE I. Percentages of area reduction stenosis differences with respect to the ground true values evaluated by 3D ultrasonography (positive and negative signs indicate, respectively, an overestimation or underestimation of the stenosis severity): (a) using the mechanical linear scanning method and (b) using the freehand scanning method for the reference phantom, the Palmaz phantom, and the Boston Scientific phantom. The ground true percentages of area reduction stenosis for S1 and S2 were 75% and 80%, respectively. The stents covered the S2 stenosis. There were statistically significant differences ($\alpha, \beta, \gamma, \delta$) based on the ANOVA statistical test (Tukey method for multiple comparisons), $p < 0,05$. α represents a significant difference with the corresponding stenosis of the reference phantom using the same scanning method for the corresponding imaging mode; β represents a significant difference with the corresponding stenosis of the Palmaz and Boston phantoms using the same scanning method for the corresponding imaging mode; γ represents a significant difference with the corresponding stenosis for the freehand mode and the linear scanning method; δ represents a significant difference between B mode and power Doppler on the corresponding stenosis using the same method.

		(a) Linear scanning method		(b) Freehand method	
		B mode (%)	Power Doppler (%)	B mode (%)	Power Doppler (%)
Reference phantom	S1	0.1 ± 0.6	$-1.8 \pm 0.7^\delta$	1.3 ± 1.0	-0.8 ± 3.1
	S2	0.6 ± 0.4	$-3.2 \pm 1.0^\delta$	-0.4 ± 1.2	-2.7 ± 3.2
Boston phantom	S1	1.3 ± 1.0	$0.1 \pm 1.5^\delta$	2.4 ± 1.5	$0.1 \pm 1.8^\beta$
	S2	$-2.6 \pm 2.0^{\alpha,\beta}$	$7.0 \pm 1.3^{\alpha,\delta}$	$-6.2 \pm 3.2^{\alpha,\gamma}$	$2.0 \pm 2.5^{\alpha,\beta,\gamma}$
Palmaz phantom	S1	1.7 ± 2.2	$-1.5 \pm 4.2^\delta$	2.5 ± 1.4	$-6.7 \pm 4.1^{\alpha,\delta,\gamma}$
	S2	$-6.2 \pm 2.5^\alpha$	$5.6 \pm 5.8^{\alpha,\delta}$	$-4.2 \pm 3.0^\alpha$	$6.2 \pm 6.4^\alpha$

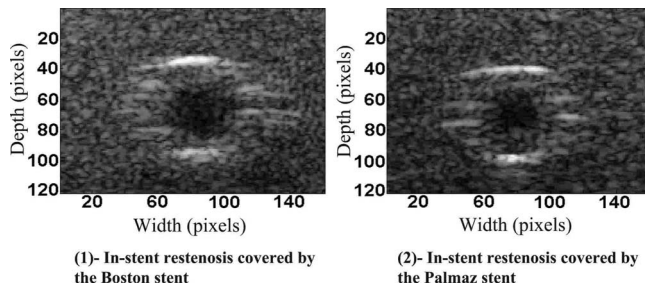


Fig. 9. Two-dimensional U.S. images of the in-stent restenosis covered by (1) the Boston stent and (2) the Palmaz stent.

Boston phantom was, respectively, evaluated with 7% and 2% errors by both scanning methods ($p < 0.05$).

IV. DISCUSSION

IV.A. 3D B-mode imaging is accurate in detecting stenoses but underestimates the severity of in-stent restenoses

Recently, Barratt *et al.*¹² acquired combined B-mode and PDA cross-sectional images of a tissue-mimicking *in vitro* carotid artery bifurcation under pulsatile flow. The 3D free-hand reconstruction (pcBird, Ascension Technology Corporation, Burlington, VT) of a 30% diameter reduction stenosis was quantified with errors between $-3.5(\pm 5.6)\%$ and $-5.1(\pm 5.6)\%$ and a 70% diameter reduction stenosis with errors from $-1.2(\pm 9.8)\%$ to $-6.5(\pm 9.9)\%$. Compared to Barratt *et al.*, we quantified tighter but geometrically simpler stenoses with similar accuracies in B mode but with smaller standard deviations. Despite imaging artifacts produced by the presence of a stent (e.g., see Figs. 5 and 9), both in-stent stenoses could be accurately quantified using 3D B-mode imaging. However, the quantification errors were greater ($p < 0.05$) with the ferromagnetic closed cell stent (Palmaz) than with the nonferromagnetic open cell prosthesis (Boston Scientific). The free cell area was lower for the Palmaz stent; this could explain why U.S. imaging artifacts produced by beam reflection and distortion seemed to be more important. Therefore, the arterial lumen of the in-stent stenosis was more difficult to segment with this stent and the largest biases and variabilities (standard deviations) were noted when using the automated fast-marching segmentation method.

IV.B. 3D PDA imaging underestimates stenoses but overestimates the severity of in-stent restenoses

The efficiency of PDA using a step motor fixed to the U.S. probe (linear scan)^{8,11} has been proven in the context of *in vitro* 3D stenosis evaluation. Using the linear scanning method, the present study underestimates severe stenoses (75% and 80% stenoses) by a maximum of 3.2% (S2 of the reference phantom). In previous studies that used a step motor for data acquisition, severe stenoses (80% area reduction stenosis) were quantified with an underestimation of 10%, 8.3%,⁸ or $2(\pm 1)\%$,¹¹ which is consistent with the present study. On the other hand, a 70° Doppler angle, as usually

used in clinic, did not always allow visualization of the flow inside in-stent restenoses probably because U.S. beam distortion artifacts are amplified at oblique angles. This fact determined the choice of an 80° Doppler angle even though it may have induced a loss of signal near the vessel wall because the Doppler shift was low and cut by the wall filter. This can explain the statistically significant underestimation of the degree of stenosis with PDA (when there was no stent). For instance, because of flow acceleration within each stenosis, the velocity components eliminated by the wall filter were more important for the normal V1 section of the vessel than within the throat of the stenosis. Each stenosis thus appeared relatively bigger in area when compared to V1. At the opposite, in-stent restenoses were overestimated using PDA no matter which stent was used because flow components were lost because of U.S. beam reflection by stent struts.

IV.C. Comparison with other imaging modalities

To our knowledge, no study reported quantitative results on in-stent restenoses evaluated with 3D ultrasound, which limits the possibility to compare our results. However, this has been the objective of some studies based on magnetic resonance angiography (MRA) and computed tomography angiography (CTA). A 50% *in vitro* nitinol in-stent restenosis was overestimated by 3.6%–9.5% in MRA and by 0.1%–7.4% in CTA.⁴ A study by Seifarth *et al.*²⁴ showed that the visualization and quantification of in-stent lumen diameter improved using a 64-slice versus 16-slice CTA. Rist *et al.*²⁵ recently investigated the use of the ultrahigh-resolution mode of a 64-slice CT scanner and quantified *ex vivo* a 2.5 mm diameter coronary artery stent (measurement of the outer diameter of the stent's artifact with a maximum overestimation of 0.13 mm). However, multislice CT remains less accurate than intravascular U.S. (IVUS).²⁶ In this last study, the maximum in-stent lumen diameter quantification error was 0.2 mm with IVUS and 1.2 mm with 16- and 64-slice CTA. Another *in vitro* study by Hamer *et al.*⁵ quantified with MRA in-stent restenosis within ten nitinol stents on an iliac artery with errors ranging from 1.1% to 8.2%. For comparison, using both scanning methods and imaging modes, the present study showed a maximum in-stent stenosis quantification error of 7%, which corresponds to a diameter quantification error of 0.55 mm.

According to the present study based on 3D B-mode and 3D PDA imagings, in-stent stenosis was evaluated with accuracies comparable to 3D MRA and CTA. However, the comparison between these imaging modalities is limited because different kinds of stents were used (dimensions, mesh characteristics, materials). Indeed, we observed significant differences when scanning with U.S. the prototype Boston Scientific and commercially available Palmaz stents.

Recent clinical reports have addressed the issue of redefining duplex U.S. velocity criteria to diagnose in-stent restenoses.^{27,28} Indeed, new PSV and PSV ratio thresholds were proposed to diagnose mild-to-moderate and moderate-to-severe in-stent lesions. When compared to stenoses with

similar angiographically based severities, duplex U.S. tends to overestimate the importance of the vessel narrowing. Several hypotheses were proposed to explain this finding. Most authors believe that the apparent velocity increase may be related to decreased compliance and elasticity of the artery following stent placement, which implies that the energy normally applied to dilate the artery is now used to increase velocities.²⁸ An *in vitro* flow modeling study also suggested that the stent placement across the carotid bifurcation and stent design could induce alterations in the flow characteristics.²⁹ Although speculated as having no impact on biased Doppler velocity estimates,³⁰ *in vitro* flow phantom data clearly proved that the stent material and characteristics induce U.S. image artifacts.³¹ In this last study, by using a constant pulsatile flow and ovine internal carotid arteries, either an increase, no effect, or a decrease in flow velocities was noted when measurements were performed across the stent (11 stents were tested, each having the same deployed dimension). Similar to our conclusion, alterations of U.S. signals by the stent struts and potential impacts of the strut thickness, opening size, shape, geometry, and stent material may all likely contribute to U.S. echo artifacts.³¹

IV.D. Impact of the linear versus freehand scanning method

According to Table I, 3D freehand U.S. was less accurate than the linear scanning method ($p < 0.05$). This can be attributed to errors inherent to the 3D freehand U.S. system.³² Namely, errors arise during registration of spatial positions with the tracking device, during calibration with the planar phantom (Plexiglas plate), and during 3D reconstruction, which is more complicated than linear scans where simple stacking of images was done. As an example, errors are introduced by the temporal calibration (executed by STRADWIN), where the acquisition of an image with its position (given by Fastrak) may not accurately be synchronized. The calibration strategy with a planar phantom that gave an accuracy of 1 mm in this study could have been improved because it gives little information on rotation parameters (for the calibration matrix). Better results would have probably been obtained by using a cross wire or a Z-fiducial calibration phantom.³³ Finally, errors can come from the magnetic tracking device that is sensitive to surrounding ferromagnetic metals. Indeed, we observed an impact of the type of stent based on the analysis of variance and multiple pairwise comparisons revealed larger area reduction stenosis differences for the ferromagnetic Palmaz stent, namely, in B mode for the linear scanning method and PDA for the freehand scanning mode. In addition to errors due to the reverberation of the stent cells, a magnetostrictive coupling between U.S. waves and the magnetic field generated by the Fastrak could happen in ferromagnetic metals and cause ultrasound attenuation. This attenuation is higher in ferromagnetic metals than in nonferromagnetic ones.^{34,35}

IV.E. Limitations of the study

Several types of tracking device have been proposed and used for 3D U.S. imaging (e.g., magnetic, mechanical, optical, acoustical, hybrid). Our freehand U.S. results could have been improved with optical tracking systems, which have lower rms errors than electromagnetic systems. For comparison, the accuracy reported by manufacturers is approximately 0.15 mm rms for optical tracking (Optotrack 3020, Northern Digital Inc., Toronto, ON, Canada) as opposed to 0.76 and 1.2 mm rms for the magnetic Fastrak and Flock of Birds (Ascension Technology Corporation, Burlington, VT) systems, respectively. However, optical systems are expensive and their use in a clinical environment is limited since the sensor-transmitter line of sight cannot be interrupted.

It is anticipated that additional reconstruction errors would occur for *in vivo* acquisitions³⁶ since movement artifacts can appear when the acquisition is performed with a patient. In addition, blood flow pulsatile movements might also cause artifacts. We recognize that a high steady flow rate was selected in this study (500 ml/min), which may have improved our PDA results because the impact of the wall filter on flow removal near the vessel wall was reduced. Note, however, that this flow rate is representative of reported values for femoral arteries (100–660 ml/min according to Vääntinen³⁷). Smaller flow rates are typically found in internal carotid arteries (≈ 200 ml/min).³⁸ Refraction of the U.S. beam and changes in the speed of sound as the pulse travels inside the human body can as well create 3D reconstruction errors. Clinical validations would be required to establish the reliability of this imaging modality.

In this study, the accurate quantification of stenoses as well as the small errors reported in the case of in-stent restenoses using 3D U.S. are in part attributed to the accuracy of the segmentation algorithm and to the use of a 10 MHz probe. Indeed, others used 4 MHz (Refs. 8 and 11) or 5 MHz (Ref. 8) probes that have lower spatial resolutions. Note that the segmentation algorithm is currently not commercially available.

V. CONCLUSION

In this study, in-stent stenosis quantification was done using 3D freehand ultrasound with a maximum error of 6.2% both in B mode and PDA (Table I). This is in the range of errors obtained with MRA and CTA for similar experimental setup.^{4,5} Thus, the convenient 3D freehand U.S. method (compared to linear scan) is considered, based on our study, good enough to be a feasible method for vascular imaging and quantification of in-stent restenoses. However, more studies should be performed to compare the *in vivo* quantification accuracy of in-stent restenosis between 3D ultrasound and other imaging modalities.

ACKNOWLEDGMENTS

Thanks to Boston Scientific (Munich, Germany) for the donation and for letting the authors use their prototype stent, to Dr J. de Guise from the Laboratoire d'imagerie ortho-

pédique of the Research Center of the University of Montreal Hospital for the loan of the Fastrak (Polhemus) tracking device, to Ms I. Renaud for her help during data acquisition, and to Dr F. Destrempe for his mathematical advices. This work was supported by the Canadian Institutes of Health Research (CIHR) under MOP Grant No. 53244. Dr. Soulez and Dr. Cloutier are, respectively, recipient of a Clinical Research Scholarship Award and of a National Scientist Award of the Fonds de la Recherche en Santé du Québec. Ms. Lécart was recipient of a Studentship Award of the Institut de Génie Biomédical (IGB), University of Montreal.

- ^{a)} Author to whom correspondence should be addressed. Electronic mail: guy@cloutier.umontreal.ca; Telephone: 514-890-8000-24703; Fax: 514-412-7505.
- ¹B. K. Lal *et al.*, "Carotid artery stenting: Is there a need to revise ultrasound velocity criteria?," *J. Vasc. Surg.* **39**, 58–66 (2004).
 - ²E. I. Levy *et al.*, "Frequency and management of recurrent stenosis after carotid artery stent implantation," *J. Neurosurg.* **102**, 29–37 (2005).
 - ³S. F. Stanziale *et al.*, "Determining in-stent stenosis of carotid arteries by duplex ultrasound criteria," *J. Endovasc. Ther.* **12**, 346–353 (2005).
 - ⁴L. Létourneau-Guillon *et al.*, "CT and MR imaging of nitinol stents with radiopaque distal markers," *J. Vasc. Interv. Radiol.* **15**, 615–624 (2004).
 - ⁵O. Hamer *et al.*, "In vivo evaluation of patency and in-stent stenoses after implantation of nitinol stents in iliac arteries using MR angiography," *AJR, Am. J. Roentgenol.* **185**, 1282–1288 (2005).
 - ⁶E. M. Jung *et al.*, "B-flow and B-flow with 3D and SRI postprocessing before intervention and monitoring after stenting of the internal carotid artery," *Clin. Hemorheol. Microcirc.* **36**, 35–46 (2007).
 - ⁷A. Fenster *et al.*, "Three-dimensional ultrasound imaging of the vasculature," *Ultrasonics* **36**, 629–633 (1998).
 - ⁸Z. Guo and A. Fenster, "Three-dimensional power Doppler imaging: A phantom study to quantify vessels stenosis," *Ultrasound Med. Biol.* **22**, 1059–1069 (1996).
 - ⁹A. Fenster, D. B. Downey, and H. N. Cardinal, "Three-dimensional ultrasound imaging," *Phys. Med. Biol.* **46**, R67–R99 (2001).
 - ¹⁰A. Fenster and D. B. Downey, "3D ultrasound imaging: A review," *IEEE Eng. Med. Biol. Mag.* **15**, 41–51 (1996).
 - ¹¹G. Cloutier *et al.*, "Assessment of arterial stenosis in a flow model with power Doppler angiography: Accuracy and observations on blood echogenicity," *Ultrasound Med. Biol.* **26**, 1489–1501 (2000).
 - ¹²D. C. Barratt *et al.*, "Reconstruction and quantification of the carotid artery bifurcation from 3-D ultrasound images," *IEEE Trans. Med. Imaging* **23**, 567–583 (2004).
 - ¹³L. Allard *et al.*, "3-D power Doppler ultrasound imaging of an in vitro arterial stenosis," *Acoust. Imaging*, 267–272 (1997).
 - ¹⁴D. W. Rickey *et al.*, "A wall-less vessel phantom for Doppler ultrasound studies," *Ultrasound Med. Biol.* **21**, 1163–1176 (1995).
 - ¹⁵P. Tortoli *et al.*, "Flow imaging with pulsed Doppler ultrasound and flow phantoms," *IEEE Trans. Ultrason. Ferroelectr. Freq. Control* **46**, 1591–1596 (1999).
 - ¹⁶C. Bertolotti *et al.*, "Influence of multiple stenoses on echo-Doppler functional diagnosis of peripheral arterial disease: A numerical and experimental study," *Ann. Biomed. Eng.* **34**, 564–574 (2006).
 - ¹⁷B. Robert, "Échographie tridimensionnelle," Ph.D. thesis, Université Paris Descartes, Paris, France, 1999.
 - ¹⁸R. W. Prager, A. Gee, and L. Berman, "Stradx: Real-time acquisition and visualization of freehand three-dimensional ultrasound," *Med. Image Anal.* **3**, 129–140 (1999).
 - ¹⁹R. W. Prager *et al.*, "Rapid calibration for 3D freehand ultrasound," *Ultrasound Med. Biol.* **24**, 855–869 (1998).
 - ²⁰F. Rousseau, P. Hellier, and C. Barillot, "Confhuisus: A robust and fully automatic calibration method for 3D freehand ultrasound," *Med. Image Anal.* **9**, 25–38 (2005).
 - ²¹M.-H. Roy Cardinal *et al.*, "Intravascular ultrasound image segmentation: A three-dimensional fast-marching method based on gray level distributions," *IEEE Trans. Med. Imaging* **25**, 590–601 (2006).
 - ²²M. H. Roy Cardinal *et al.*, "Automatic 3D segmentation of intravascular ultrasound images using region and contour information," *Lecture Notes in Computer Science, Medical Image Computing and Computer Assisted Intervention—MICCAI 2005 Proceedings, Palms Spring, CA, 2005*, Vol. 3749, pp. 319–326.
 - ²³G. Cloutier *et al.*, "A multimodality vascular imaging phantom with fiducial markers visible in DSA, CTA, MRA and ultrasound," *Med. Phys.* **31**, 1424–1433 (2004).
 - ²⁴H. Seifarth *et al.*, "64-versus 16-slice CT angiography for coronary artery stent assessment. In vitro experience," *Invest. Radiol.* **41**, 22–27 (2006).
 - ²⁵C. Rist *et al.*, "Ultra-high-resolution mode for the assessment of coronary artery stents—Ex vivo imaging with 64-slice computed tomography," *Acad. Radiol.* **13**, 1165–1167 (2006).
 - ²⁶N. Beohar *et al.*, "Quantitative assessment of in-stent dimension: Comparison of 64 and 16 detector multislice computed tomography to intravascular ultrasound," *Catheter. Cardiovasc. Interv.* **68**, 8–10 (2006).
 - ²⁷C. Setacci *et al.*, "Grading carotid intrastent restenosis: A 6-year follow-up study," *Stroke* **39**, 1189–1196 (2008).
 - ²⁸B. K. Lal *et al.*, "Duplex ultrasound velocity criteria for the stented carotid artery," *J. Vasc. Surg.* **47**, 63–73 (2008).
 - ²⁹O. Greil *et al.*, "Flow velocities after carotid artery stenting: Impact of stent design. A fluid dynamics study in a carotid artery model with laser Doppler anemometry," *Cardiovasc. Intervent. Radiol.* **28**, 66–76 (2005).
 - ³⁰A. F. AbuRahma *et al.*, "Optimal carotid duplex velocity criteria for defining the severity of carotid in-stent restenosis," *J. Vasc. Surg.* **48**, 589–594 (2008).
 - ³¹C. Spies, R. Doshi, J. Spoon, and R. J. Snell, "Carotid artery stent type influences duplex ultrasonography derived peak-systolic velocity: Findings of an in-vitro model," *Catheter. Cardiovasc. Interv.* **70**, 309–315 (2007).
 - ³²G. M. Treece *et al.*, *Correction of probe pressure artifacts in freehand 3D ultrasound*, Proceedings of Medical Image Computing and Computer Assisted Intervention, Utrecht, The Netherlands, 2001, pp. 283–290.
 - ³³L. Mercier *et al.*, "A review of calibration techniques for freehand 3D ultrasound systems," *Ultrasound Med. Biol.* **31**, 143–165 (2005).
 - ³⁴M. J. W. Povey, D. J. Meredith, and E. R. Dobbs, "Electromagnetic generation and attenuation of ultrasound in ferromagnetic metals. I.," *J. Phys. F: Met. Phys.* **10**, 2041–2053 (1980).
 - ³⁵M. J. W. Povey, D. J. Meredith, and E. R. Dobbs, "Electromagnetic generation and attenuation of ultrasound in ferromagnetic metals. II.," *J. Phys. F: Met. Phys.* **10**, 2555–2572 (1980).
 - ³⁶E. I. Bluth *et al.*, "Power Doppler imaging: Initial evaluation as a screening examination for carotid artery stenosis," *Radiology* **215**, 791–800 (2000).
 - ³⁷E. Vääntinen, "Electromagnetic measurement of the arterial blood flow in the femoropopliteal region," *Acta Chir. Scand.* **141**, 353–359 (1975).
 - ³⁸J. C. Greenfield, Jr. and G. T. Tindall, "Effect of norepinephrine, epinephrine, and angiotensin on blood flow in the internal carotid artery of man," *J. Clin. Invest.* **47**, 1672–1684 (1968).